
The Nonlinearity Coefficient

- Predicting Overfitting in Deep Neural Networks

George Philipp*, Jaime G. Carbonell
Carnegie Mellon University
Pittsburgh, PA 15213
george.philipp@email.de; jgc@cs.cmu.edu

Abstract

For a long time, designing neural architectures that exhibit high performance was considered a dark art that required expert hand-tuning. One of the few well-known guidelines for architecture design is the avoidance of exploding gradients, though even this guideline has remained relatively vague and circumstantial. We introduce the nonlinearity coefficient (NLC), a measurement of the complexity of the function computed by a neural network that is based on the magnitude of the gradient. Via an extensive empirical study, we show that the NLC is a powerful predictor of test error and that attaining a right-sized NLC is essential for optimal performance.

The NLC exhibits a range of intriguing and important properties. It is closely tied to the amount of information gained from computing a single network gradient. It is tied to the error incurred when replacing the nonlinearity operations in the network with linear operations. It is not susceptible to the confounders of multiplicative scaling, additive bias and layer width. It is stable from layer to layer. Hence, we argue that the NLC is the first robust predictor of overfitting in deep networks.

1 Introduction

Designing neural architectures that perform well can be a difficult process. In particular, the exploding gradient problem has been a major challenge for training very deep neural networks at least since the advent of gradient-based parameter learning [8, 18, 19]. However, there is still no consensus about which metric should be used for determining the presence of pathological exploding gradients. Should we care about the length of the gradient vector [14]? Should we care about the size of individual components of the gradient vector [12, 33, 38]? Should we care about the eigenvalues of the Jacobian [26, 27, 32]? Depending on the metric used, different strategies arise for combating exploding gradients. For example, manipulating the width of layers as suggested by e.g. [13, 39] can greatly impact the size of gradient vector components but tends to leave the length of the entire gradient vector relatively unchanged. The popular He initialization for ReLU networks [14] is designed to stabilize gradient vector length, whereas the popular Xavier initialization for tanh networks [12] is designed to stabilize the size of gradient vector components. While there is much evidence that gradient explosion when defined according to some metrics is associated with poor performance when certain architectures are paired with certain optimization algorithms (e.g. [12, 33]), it is often unclear how to generalize those results.

Recently, [29] demystified many issues surrounding the exploding problem. They introduce the *gradient scale coefficient (GSC)*, the first metric for determining the presence of pathological exploding gradients that can be shown to directly lead to training difficulties. They also introduced the *collapsing domain problem*, where hidden layer activations corresponding to different datapoints become more and more similar with depth. Building on these ideas, we make the following contributions.

*corresponding author

1. We introduce the *nonlinearity coefficient (NLC)*, a measurement of the combined pathology of exploding gradients and collapsing domain.
2. We verify that the NLC is an accurate estimate of the amount of information gained from computing a single gradient of a neural network, and therefore of the complexity of the function computed by the network.
3. Via an extensive empirical study of more than 15,000 full training runs, we show that the NLC is a powerful predictor of test error and that attaining a right-sized NLC is essential for optimal performance, at least in fully-connected feedforward networks.
4. Through the same study, we uncover the necessity of avoiding excessively biased neuron activations, and highlight the power of skip connections for reducing the NLC and attaining additional performance gains.
5. We detail an intriguing relationship between the NLC and the degree to which the nonlinearities used in a network can be approximated by linear functions.
6. We demonstrate that, by design, the NLC is not susceptible to the confounders of multiplicative scaling, additive bias and layer width. We argue that this makes the NLC the best current single predictor of network performance in general, and overfitting in particular.

2 Notation and Terminology

We define a neural network f as a succession of layers f_l , $1 \leq l \leq L$. Each layer outputs a vector of dimensionality d_l , which is fixed for each layer but may vary between layers. Each layer consumes one or more outputs of previous layers as inputs. The lowest layer, f_1 , consumes the input x , a vector of fixed dimensionality d . We also denote x by f_0 and d by d_0 . We assume a prediction framework, where the output layer f_L is considered to output the prediction of the network and the goal is to minimize the value of the ‘error function’ e over the network’s prediction and the true label y , in expectation over some data distribution \mathcal{D} .

$$\begin{aligned} \hat{\theta} &= \arg \min_{\theta} \mathbb{E}_{(x,y) \sim \mathcal{D}} [e(f(\theta, x), y)] & f(\theta, x) &= f_L \\ f_l &= f_l(\theta_l, f_{k_l(1)}, \dots, f_{k_l(I_l)}) \text{ for all } 1 \leq l \leq L & f_0 &= x \end{aligned}$$

k_l represents the vector of the layer indices layer l takes as input, and I_l is the number of inputs. Each layer is associated with a trainable parameter sub-vector θ_l that collectively make up the parameter vector $\theta = (\theta_1, \dots, \theta_L)$. We denote the error function e also by f_{L+1} and set $d_{L+1} = 1$. Let $\mathcal{J}_k^l(\theta, x, y)$ be the Jacobian of the l ’th layer f_l with respect to the k ’th layer f_k evaluated with parameter θ at (x, y) , where $0 \leq k \leq l \leq L + 1$. In our notation, we often omit dependencies on x, y and θ for brevity and readability and simply write, for example, \mathcal{J}_k^l . We also shorten the gradient of the error \mathcal{J}_l^{L+1} to g_l . $f_l(j)$ and $g_l(j)$ denote the j ’th entry of f_l and g_l respectively, where $1 \leq j \leq d_l$. Denote the standard deviation of a random variable X as $\mathbb{S}[X]$. Finally, let the ‘quadratic expectation’ \mathbb{Q} of a random variable X be defined as $\mathbb{Q}[X] = \sqrt{\mathbb{E}[X^2]}$, i.e. the generalization of the quadratic mean to random variables.

3 On the complexity of neural networks - deriving the NLC

Background Recently, [29] introduced a rigorous measurement for the presence of pathological exploding gradients, the gradient scale coefficient.

Definition 1. The *gradient scale coefficient (GSC)* of a network f with respect to layers k and l , parameter value θ , input x and label y is $GSC(k, l, f, \theta, x, y) := \frac{\|\mathcal{J}_k^l(\theta, x, y)\|_F \|f_k(\theta, x, y)\|_2}{\sqrt{d_k} \|f_l(\theta, x, y)\|_2}$

Specifically, the GSC of the error is $GSC(l, L + 1) = \frac{\|g_l\|_2 \|f_l\|_2}{\sqrt{d_l} e}$. [29] showed how a large GSC directly leads to training difficulty and high errors. The crucial insight is that as the GSC increases, the information that is gained from computing a single gradient of the network decreases. Consider some value F_l taken by layer f_l and some perturbation $\delta = \epsilon u \|F_l\|_2$ of that value,

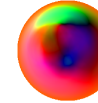
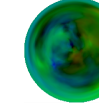
L	batchnorm ReLU			plain ReLU			
	2	10	50	2	10	50	
$GSC(0, L)$	1.23	5.8	8200	0.96	0.98	1.55	
$DBC(L)$	1	1	1	1.24	2.6	3.79	
$NLC(0, L)$	1.23	5.8	8200	1.21	2.58	5.94	
Illustration							

Table 1: GSC, DBC and NLC for two architectures at different depths. Note that the rightmost color plot is a contrast-heightened version of the plot to its left.

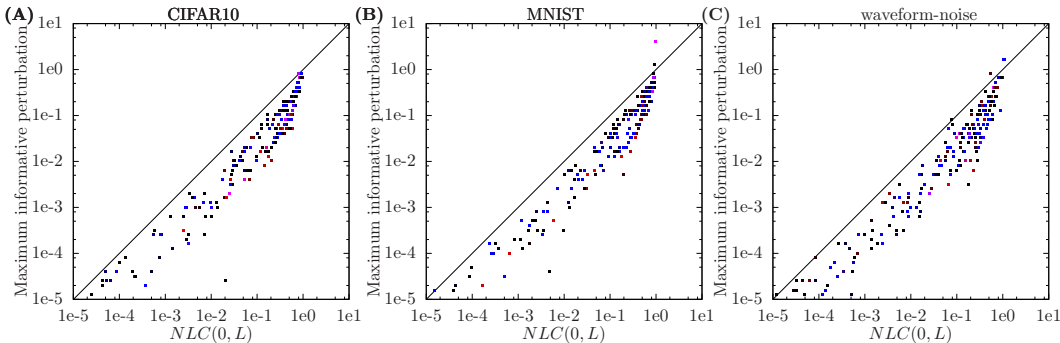


Figure 1: Relationship between the NLC and the relative size of the region in which the gradient is informative in a random direction. The more red a point is, the higher $DBC(L)$. The bluer a point is, the stronger the skip connections.

where $u \sim U$ and U is the uniform distribution over unit length vectors. Then $GSC(l, L + 1) = \lim_{\epsilon \rightarrow 0} \frac{1}{e(F_l)\epsilon} \mathbb{Q}_u[e(F_l + \delta) - e(F_l)]$. In plain language, a random change to F_l of relative size $\frac{1}{GSC(l, L+1)}$ leads to a change in the error of quadratic expectation $e(F_l)$ according to the local linear approximation induced by the network gradient. However, this means that the value of the linear approximation of the error becomes negative with significant probability, which is unrealistic. Therefore, $\frac{1}{GSC(l, L+1)}$ is a bound on the relative size of the region in which the gradient of the network is informative, i.e. the fraction of the signal F_l that can be corrupted before the gradient becomes uninformative. In yet other words, as the GSC increases, the relative size of the region that satisfies the first Wolfe condition shrinks proportionally [37]. In this sense, the GSC measures the complexity of the neural network. [29] showed how this complexity ultimately leads to poor outcomes by reducing effective depth [36].

[29] also introduced the *collapsing domain problem*, where latent representations corresponding to different datapoints become more and more similar with depth. In the analysis above, we found that the informativeness of the gradient scales inversely with $e(F_l)$, because this value denotes the distance to the boundary of the domain of the error function in a descent direction. [29] generalized this principle to the intermediate representations of the network. As latent representations become more similar, their domain shrinks and thus the distance to the domain boundary shrinks, and thus the informativeness of the gradient of those representations with respect to lower layers shrinks as well.

Defining the NLC We now make a crucial modelling assumption. We assume that the distribution of f_l as (x, y) vary in \mathcal{D} is a Gaussian distribution with covariance matrix $\sigma_l I$ for some constant σ_l and the identity matrix I . In that case, the relative shrinkage of the domain is simply the ratio of the size of the latent representations and σ . We estimate both quantities empirically and thus define:

Definition 2. The *domain bias coefficient (DBC)* of network f at layer l with respect to \mathcal{D} and θ is
$$DBC(l, f, \theta, \mathcal{D}) := \frac{\mathbb{Q}_{j \in \mathcal{D}} f_l(j, \theta, x, y)}{\mathbb{Q}_j \mathbb{S}_{\mathcal{D}} f_l(j, \theta, x, y)}$$

Finally, we notice that this allows us to combine the effects of domain collapse and gradient explosion in a single metric.

Definition 3. The *nonlinearity coefficient (NLC)* of a network f at layers $0 \leq k \leq l \leq L + 1$ with respect to \mathcal{D} and θ is $NLC(k, l, f, \theta, \mathcal{D}) := \frac{\mathbb{Q}_{\mathcal{D}} \|\mathcal{J}_k^L(\theta, x, y)\|_F \mathbb{Q}_{\mathcal{D}} f_k(i, \theta, x, y)}{\sqrt{d_i} \mathbb{Q}_{\mathcal{D}} f_i(j, \theta, x, y)}$.

We obtain $NLC(k, l) = GSC(k, l) \frac{DBC(l)}{DBC(k)}$ if we place $\mathbb{Q}_{\mathcal{D}}$ terms appropriately in $GSC(k, l)$. Effectively, we augment the GSC with a more accurate, though potentially less conservative, estimate of the size of the domain. We illustrate the GSC , DBC and NLC in table 1. We plot their values for various architectures, together with a color map of the function computed by the network on a subspace of the input space, where different colors correspond to different regions of the output space. As depth grows, the GSC of a batchnorm-ReLU network grows but the DBC is constant. Therefore, the informativeness of the gradient decreases, but all regions / colors of output space are still present. In contrast, for an un-normalized ReLU network, the DBC grows more quickly. Therefore, the output oscillates in a small, biased region of output space. The NLC combines and captures both effects.

Empirical study We verified experimentally that the NLC captures gradient informativeness in practice. We sampled a large number of neural architectures at random. We varied the depth of the network, the scale of initial weights, scale of initial bias, nonlinearity, normalization method, presence of skip connections, location of skip connections and strength of skip connections. We chose from a set of 8 nonlinearities (table 2), which were further modified by random dilation, lateral shift and debiasing. However, we only considered fully-connected feedforward networks, as is (perhaps unfortunately) common in analytical studies of deep networks (e.g. [7, 30, 31, 33]). See the appendix for the full details of our architecture sampling scheme as well as all experiments conducted for this study. We studied three datasets: MNIST, CIFAR10 and waveform-noise. The latter is from the UCI repository of datasets popular for evaluating fully-connected networks [22]. Again, see the appendix for details.

We sampled 250 architectures for each dataset and computed both $NLC(0, L)$ as well as the median of the relative size of the region in input space where the local linear approximation was informative in a random direction. See figure 1 for the results. Indeed, there is a close relationship between both quantities.

4 The predictive power of the NLC - 3 rules for architecture design

We then proceeded to train each of our 750 architectures with SGD. We performed an extensive independent grid search for each architecture to determine the optimal step size, thereby eliminating this potential confounder. This led to a total of over 15,000 full training runs. [29] demonstrated the importance of setting step sizes independently for each architecture.

In figure 2, we plot $NLC(0, L)$ against the test error for each architecture, where the test error was taken after training with the step size that achieved the lowest validation error. We find that for all three datasets, the test error is highly related to the NLC . In fact, for NLC s in a range between 1 and 100 (figures B/D/F), the test error seems to be bounded below by a linear function of the NLC . For all three datasets, the optimal performance can only be obtained when the NLC is in a narrow range, approximately between 1 and 2. We also observe that most of our random architectures have an NLC greater than the optimal value. In other words, it is very easy to overfit. Hence, we state our first rule for neural architecture design.

Rule 1. Choose a neural architecture that has an ideal complexity level, as measured by $NLC(0, L)$.

Note that the NLC is cheap to compute. Throughout this study, we compute it via a single pass over the dataset in the initialized state, and also approximate $\mathbb{Q}_{\mathcal{D}} \|\mathcal{J}_0^L\|_F$ by $\sqrt{d_L} \frac{\mathbb{Q}_{\mathcal{D}} \|g_0\|_2}{\mathbb{Q}_{\mathcal{D}} \|g_L\|_2}$. In figure 3A, we show the NLC for CIFAR10 before training against the NLC after training. In the vast majority of cases, the change is small. In figure 2 A/C/E, we notice that there are a few outliers in the top left corner which represent untrainable architectures that had random performance after training. We color-coded the points in figure 2, where the more red a point is, the higher $DBC(L)$. We find that the aforementioned outliers correspond to the architectures that exhibit the highest bias. To further investigate this effect, we modified our CIFAR10 architectures so that they are likely to yield higher

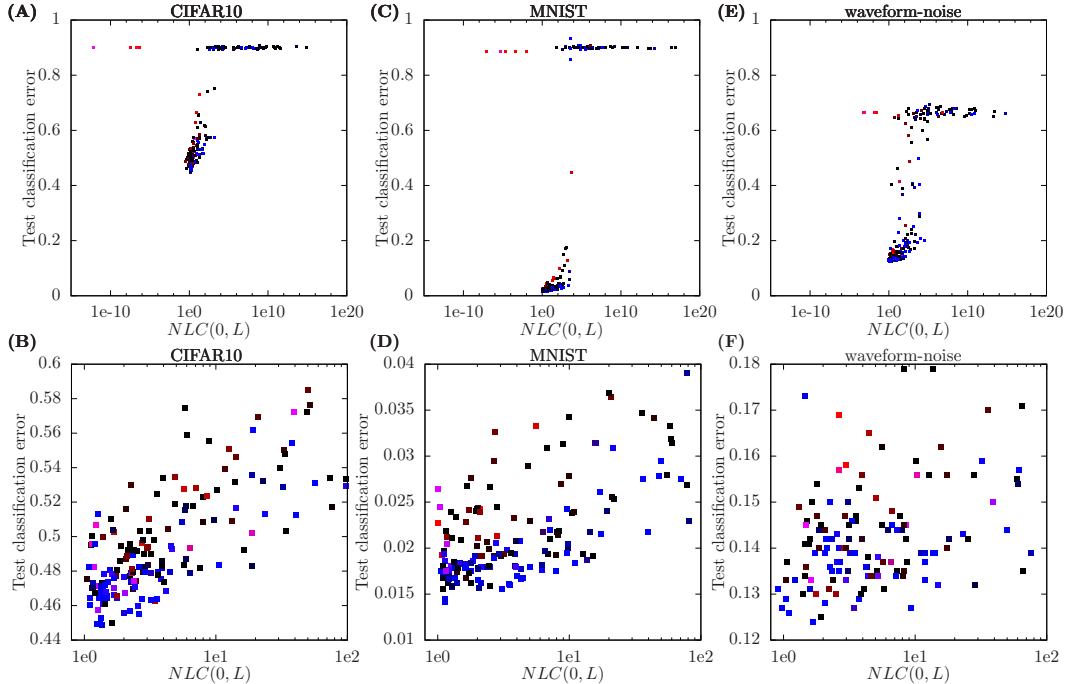


Figure 2: Relationship between the NLC and test error. The more red a point is, the higher $DBC(L)$. The bluer a point is, the stronger the skip connections.

domain bias values. See the appendix for details. We trained those architectures and plot $DBC(L)$ versus test error in figure 3B. While bias does not seem to affect performance much up to a certain point, all architectures with a DBC beyond 300 exhibit random performance. Hence, we state our second rule for neural architecture design.

Rule 2. Avoid an excessively high bias, as measured by $DBC(L)$.

[29] detailed the *k-dilution* effect, which causes skip connections such as those employed in ResNet [15] to drastically reduce the growth of the GSC during backpropagation. Further, they demonstrated that ResNets approximately achieve an *orthogonal initial state* and argue that this leads to performance gains beyond just reducing complexity. In figure 2, we color points so that the stronger the skip connections of an architecture, the more the point is blue. Architectures without skip connections have no blue color. As expected, we find that architectures with skip connections exhibit lower NLC’s and tend to outperform other architectures with comparable NLCs. Hence, we formulate our third rule.

Rule 3. Utilize skip connections to reduce the NLC and to achieve additional test error gains.

All of our networks were thus far trained with SGD. Adam [21] is an optimization algorithm that, among other things, scales down large gradients that arise in lower layers in many architectures with high NLCs. [29] argued that the training difficulty incurred by a high GSC, and hence high NLC, cannot be overcome with gradient-based optimization schemes as they are caused by an inherent lack of informativeness of the gradient. We re-trained our 250 waveform-noise architectures with Adam. The results are shown in figure 3C. The relationship between NLC and test error is indeed largely unchanged compared to figure 2C.

5 On the NLC and the linear approximability of nonlinearities

In this section, we expose the connection between the NLC and low-level properties of the nonlinearities the network uses. Given a 1d nonlinearity operation τ and pre-activations distributed according to a Gaussian with mean 0 and standard deviation σ , we set

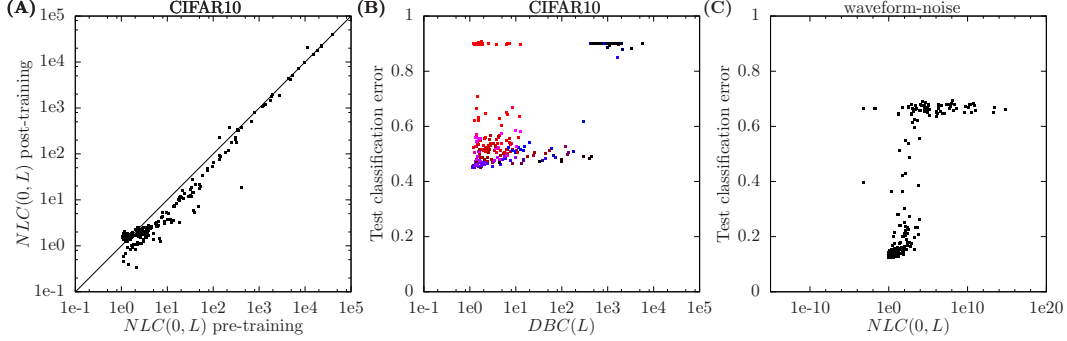


Figure 3: A: NLC before vs after training. B: DBC against test error on modified architectures. The more red a point is, the higher $NLC(0, L)$. C: NLC against test error. Networks were trained with Adam.

$$NLC_{\tau}(\sigma) = \frac{\sigma}{\mathbb{S}_{s \sim \mathcal{N}(0, \sigma)} \tau(s)} \mathbb{Q}_{s \sim \mathcal{N}(0, \sigma)} \tau'(s)$$

It is easy to check that if f_l corresponds to applying τ to each component of f_{l-1} , and f_{l-1} is distributed according to a Gaussian with mean 0 and covariance σI , then $NLC(l-1, l) = NLC_{\tau}(\sigma)$. It turns out that if batch normalization follows a fully-connected operation, the neuron activations post batchnorm are indeed approximately unit Gaussian distributed. This follows from the central limit theorem [30]. Hence, in a network containing layers of a fully-connected operation, batchnorm and a nonlinearity τ , we expect the NLC of a layer to be approximately $NLC_{\tau}(1)$, as batchnorm is approximately linear. We train a 2-layer network with batch normalization, which contains a single nonlinearity operation at the single hidden layer. In table 2, we show $NLC_{\tau}(1)$ for all 8 nonlinearities we used, as well as the median empirical $NLC(0, L)$ value over 10 random initializations of the 2-layer networks. We find a close match between the two values. We then measure $NLC(0, L)$ in 49-layer batchnorm networks, which contain 48 nonlinearity operations. For 6 out of 8 nonlinearities, $NLC(0, L)$ closely matches the exponentiated $NLC_{\tau}(1)^{48}$. This underscores the theoretical analysis of [29] about the exponential compounding of the layer-wise GSC. It reveals that the NLC of a network is closely tied to which nonlinearity is used. Note that the reason that the NLC value of the square and odd square nonlinearities diverge from $NLC_{\tau}(1)^L$ at high depth is because those nonlinearities increase the value of large inputs but shrink the value of small inputs. This causes the length of the latent representations corresponding to different inputs to diverge with depth, destroying Gaussianity.

We then checked whether NLC_{τ} actually measures “how nonlinear” a nonlinearity is. We computed the best linear fit for each τ given unit Gaussian input and then measured the ratio of the power of the signal filtered by this best linear fit over the power of the signal preserved. We find that for the 5 nonlinearities with the lowest NLCs, there is a close correspondence, in that this linear approximation error is around $NLC_{\tau}(1) - 1$. While this relationship breaks down for the three most nonlinear τ ’s (even tanh, Gaussian and square), their linear approximation error still exceeds those of the other 5 nonlinearities. We conclude that NLC_{τ} , and hence $NLC(0, L)$, is a “true” measure of nonlinearity.

These insights also imply that the NLC can be managed by changing the linear approximability of nonlinearities. For all CIFAR10 architectures that exhibited an $NLC(0, L)$ greater than 10, we replaced the nonlinearity $\tau(s)$ by $0.1\tau(s) + 0.9s$, i.e. we heavily diluted the nonlinearity with a linear function. We retrained those architectures and obtained a performance improvement in 102 out of 110 cases. This shows that the NLC is much more important to the performance of the network than the precise shape of the nonlinearity.

6 On the robustness of the NLC vs other metrics

In this section, we discuss how the NLC fares against other popular or recently proposed measures of network trainability: the size of gradient vector components, correlation information preservation, and depth.

	ReLU	SELU[22]	tanh	sigmoid	even tanh	Gaussian	square	odd square
Formula	$\max(s, 0)$	2	$\tanh(s)$	$\frac{1}{1+e^{-s}}$	$\tanh(s)$	$\frac{1}{\sqrt{2\pi}} e^{-\frac{s^2}{2}}$	s^2	$s * s $
Illustration								
$NLC_\tau(1)$	1.211	1.035	1.085	1.017	2.335	1.577	1.414	1.155
BN $L = 2$	1.22	1.05	1.09	1.03	2.34	1.61	1.48	1.20
Lin. app. err.	0.222	0.030	0.075	0.0024	0.276	0.155	2.000	0.178
$NLC_\tau(1)^{48}$	9793	5.21	50.19	2.25	4.76e17	3.13e9	1.67e7	1009
BN $L = 49$	7376	7.06	59.9	3.06	4.90e17	3.74e9	4.28e12	1.38e11

Table 2: Nonlinearities used in this study with important metrics. Row 4 contains $NLC(0, L)$ for a 2-layer batchnorm network. Row 5 contains the linear approximation error. Row 7 contains $NLC(0, L)$ for a 49-layer batchnorm network.

Gradient vector component size Historically, there has not been a well-accepted metric for determining the presence of pathological exploding gradients. Recently, [12, 33, 38] used the magnitude of gradient vector components for this job. We paraphrase this metric as $\mathbb{Q}_{\mathcal{D},j}g_l(j)$ and abbreviate it as $GVCS(l)$. This metric has at least two drawbacks that render it unreliable in practice.

The first drawback is that a high degree of nonlinearity and resulting poor performance can be masked by simple multiplicative rescaling. Assume we are using a network that employs normalization such as batchnorm or layer norm [6]. Then the scale of the input data is largely irrelevant to the learning dynamics of the network. Yet, multiplying the input data with a constant c would cause the gradient to shrink by c as it passes through the first normalization operation. Hence, we can obtain arbitrary values of $GVCS(0)$ simply by changing the scale of the input data, without altering the trainability of the network. Therefore $GVCS(0)$ cannot directly predict trainability. This drawback shows up in even more insidious ways. Consider plain He-initialized [14] ReLU networks. Such networks exhibit a stable activation size in the forward pass and a stable gradient size in the backward pass. Yet both $DBC(L)$ and $NLC(0, L)$ converge to infinity as depth increases. In fact, the gradient is stable because the increase in complexity is exactly “offset” by the multiplicative downscaling of the domain size. Hence, $GVCS$ depicts very deep He-initialized plain ReLU networks as “perfect architectures” that avoid both exploding and vanishing gradients, yet those networks are untrainable. This drawback also affects the Lipschitz constant, another popular metric [10].

The second drawback is that a high degree of nonlinearity can also be masked by a high width. If the dimensionality of the input grows by a constant c , under most initialization schemes, the scale of initial weights in the first layer declines by \sqrt{c} , and then so does $GVCS(0)$. Hence, again, we can completely control $GVCS(0)$ by manipulating input dimensionality without affecting the trainability of the network. No matter how much the gradient grows during backpropagation, there exists an input dimensionality that masks this growth.

Even if neither layer width nor multiplicative scaling confounds $GVCS(0)$, gradient size can still vary spuriously and wildly from layer to layer and from operation to operation, which can be confusing to practitioners. Consider a batchnorm ReLU network where the weights and biases have been initialized to large values. Because of the presence of batch normalization, the initial scale of weights and biases does not impact trainability at all, as each batchnorm operation removes both effects. In figure 4, we compare $GVCS(l)$ and $NLC(l, L)$ for such a network, where width also changes drastically from layer to layer. Whereas $GVCS(l)$ goes through wild oscillations, $NLC(l, L)$ grows steadily during backpropagation according to the informativeness of the gradient.

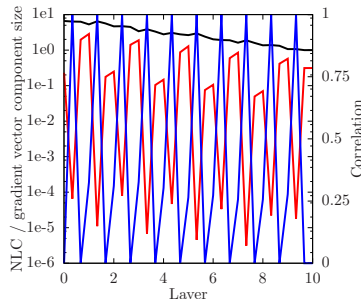


Figure 4: Comparing $GVCS(l)$ (red), $NLC(l, L)$ (black) and the correlation of latent representations corresponding to uncorrelated inputs (blue) in a depth 10 batchnorm ReLU network with large weights, large biases and oscillating width. Note that we plot the observed values after each individual linear, batchnorm and ReLU operation in the order in which they appear.

² $\mathbb{1}_{s>0}1.0507s + \mathbb{1}_{s<0}1.75814(e^s - 1)$

Correlation information [33, 38] recently proposed a new metric for predicting the trainability of deep networks: correlation information. They claim that preserving the correlation of two inputs as they pass through the network is essential for trainability. However, just as GVCS, this metric suffers from an important failure case: additive bias.

Assume we are using a network that employs batch normalization. Then biases in the features of the input do not significantly affect learning dynamics, as this bias will be filtered by the first batchnorm operation. Yet, adding a constant c to the input can arbitrarily increase correlation between inputs without affecting the correlation of the outputs. So, again, the degree of correlation change through the network can be increased arbitrarily without altering the trainability of the network.

As with the GVCS, the correlation of latent representations can vary wildly from operation to operation. In figure 4, we plot the correlation of two uncorrelated inputs as they pass through the network. As the inputs pass through the biased linear operation, correlation spikes, but this is spurious.

Depth A large body of work has detailed the benefits of depth in neural networks (e.g. [9, 11, 23, 24, 25, 34, 35]). Most of these works focus on finding specific functions which can be represented easily by deep networks, but require a prohibitively large number of neurons to represent for a shallow networks. In figure 5, we plot the test error achieved by our architectures on CIFAR10 against depth. There is virtually no pattern. If anything, the best shallow architectures outperform the best deep ones. The plot looks almost identical for the other two datasets. Of course, from a conceptual standpoint, depth cannot be used as a direct predictor of performance for all the reasons discussed throughout this section. It is important to note our deep networks were thinner than our shallow networks, as we kept the number of trainable parameters approximately constant at 1 million.

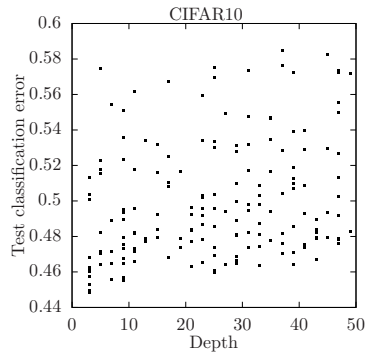


Figure 5: Depth versus test error.

We form a bold hypothesis: When fully-connected networks are applied to practical learning problems, network depth has little to no impact on performance in general beyond its indirect impact via the NLC and the total number of parameters. While we do not have enough evidence for this conclusion, we believe this is an interesting point of investigation. We have shown that the NLC is closely tied to complexity and is therefore in itself a powerful measurement of the kinds of functions a network can model.

7 Conclusion

We introduced the nonlinearity coefficient, a powerful predictor of the performance of fully-connected feedforward networks that is closely tied to the informativeness of the network gradient and the linear approximability of individual nonlinearities. Thus, the NLC represents a simple yet robust hypothesis for the complexity of a network and its likelihood to overfit. It is cheap to compute, stable throughout training and has significant practical value. We found it to be robust to basic network variations that confound other popular metrics such as gradient vector component size, correlation information, Lipschitz constant and depth. We verified our results via a large-scale empirical study that also indicates a need to avoid large biases and a desirability of skip connections to reduce the NLC and to attain further performance gains.

We found the optimal value of the NLC to be very similar between the three datasets we studied. Additionally, we also found its value to be largely independent of the input data used. Therefore, we believe the NLC could be a highly valuable data-independent filter for speeding up neural architecture search. We plan on integrating it into a large-scale search framework. Of course, we hope to extend the concepts presented in this paper to convolutional networks, which have so far largely eluded theoretical analysis based on Gaussian approximations. We are interested in studying the connection of the NLC to e.g. adversarial robustness, quantizability, sample complexity, training time and training noise. This study further underscores the need to conduct extensive, independent step size searches for each (algorithm, architecture) pair in order to obtain robust insights about deep nets, as we found that the optimal step size varied significantly between such pairs in our study. We believe that many past studies have led to spurious conclusions because of the confounder of step size bias.

References

- [1] Cifar10 dataset. <https://www.cs.toronto.edu/~kriz/cifar.html>.
- [2] Mnist dataset. <http://yann.lecun.com/exdb/mnist/>.
- [3] waveform-noise dataset. <https://archive.ics.uci.edu/ml/datasets/Waveform+Database+Generator+%28Version+1%29>.
- [4] M. Arjovsky, A. Shah, and Y. Bengio. Unitary evolution recurrent neural networks. In *ICML*, 2016. <https://arxiv.org/abs/1511.06464>.
- [5] D. Arpit, Y. Zhou, B. U. Kota, and V. Govindaraju. Normalization propagation: A parametric technique for removing internal covariate shift in deep networks. In *ICML*, 2016. <https://arxiv.org/abs/1603.01431>.
- [6] J. L. Ba, J. R. Kiros, and G. E. Hinton. Layer normalization. In *NIPS*, 2016. <https://arxiv.org/abs/1607.06450>.
- [7] D. Balduzzi, M. Frean, L. Leary, J. Lewis, K. W.-D. Ma, and B. McWilliams. The shattered gradients problem: If resnets are the answer, then what is the question? In *ICML*, 2017. <https://arxiv.org/abs/1702.08591>.
- [8] Y. Bengio, P. Simard, and F. P. Learning long-term dependencies with gradient descent is difficult. *IEEE Transactions on Neural Networks*, 5(2):157–166, 1994. <http://ai.dinfo.unifi.it/paolo/ps/tnn-94-gradient.pdf>.
- [9] M. Bianchini and F. Scarselli. On the complexity of shallow and deep neural network classifiers. In *ESANN*, 2014. <https://www.eleu.ucl.ac.be/Proceedings/esann/esannpdf/es2014-44.pdf>.
- [10] M. Cisse, P. Bojanowski, E. Grave, Y. Douphin, and N. Usunier. Parseval networks: Improving robustness to adversarial examples. In *ICML*, 2017. <https://arxiv.org/abs/1704.08847>.
- [11] O. Delalleau and Y. Bengio. Shallow vs. deep sum-product networks. In *NIPS*, 2011. <http://papers.nips.cc/paper/4350-shallow-vs-deep-sum-product-networks.pdf>.
- [12] X. Glorot and Y. Bengio. Understanding the difficulty of training deep feedforward neural networks. In *ICCV*, 2015. <http://proceedings.mlr.press/v9/glorot10a/glorot10a.pdf>.
- [13] D. Han, J. Kim, and J. Kim. Deep pyramidal residual networks. In *CVPR*, 2017. <https://arxiv.org/abs/1610.02915>.
- [14] K. He, X. Zhang, S. Ren, and J. Sun. Delving deep into rectifiers: Surpassing human-level performance on imagenet classification. In *ICCV*, 2015. <https://arxiv.org/abs/1502.01852>.
- [15] K. He, X. Zhang, S. Ren, and J. Sun. Deep residual learning for image recognition. In *CVPR*, 2016. <https://arxiv.org/abs/1512.03385>.
- [16] K. He, X. Zhang, S. Ren, and J. Sun. Identity mappings in deep residual networks. *arXiv preprint arXiv:1603.05027*, 2016. <https://arxiv.org/abs/1603.05027>.
- [17] K. Helfrich, D. Willmott, and Q. Ye. Orthogonal recurrent neural networks with scaled cayley transform. In *arXiv preprint arXiv:1707.09520*, 2017. <https://arxiv.org/abs/1707.09520>.
- [18] S. Hochreiter. Untersuchungen zu dynamischen neuronalen netzen. *Master's thesis, Technische Universität München*, 04 1991. <http://people.idsia.ch/~juergen/SeppHochreiter1991ThesisAdvisorSchmidhuber.pdf>.
- [19] S. Hochreiter and J. Schmidhuber. Long short-term memory. *Neural Computation*, 9(8):1735–1780, 1997. <http://www.bioinf.jku.at/publications/older/2604.pdf>.

- [20] S. Ioffe and C. Szegedy. Batch normalization: Accelerating deep network training by reducing internal covariate shift. In *ICML*, 2015. <https://arxiv.org/abs/1502.03167>.
- [21] D. P. Kingma and J. L. Ba. Adam: A method for stochastic optimization. In *ICLR*, 2015. <https://arxiv.org/abs/1412.6980>.
- [22] G. Klambauer, T. Unterthiner, A. Mayr, and S. Hochreiter. Self-normalizing neural networks. In *NIPS*, 2017. <https://arxiv.org/abs/1706.02515>.
- [23] J. Martens, A. Chattopadhyaya, T. Pitassi, and R. Zemel. On the representational efficiency of restricted boltzmann machines. In *NIPS*, 2013. http://www.cs.toronto.edu/~jmartens/docs/RBM_%20Representational_%20Efficiency.pdf.
- [24] H. N. Mhaskar and O. Shamir. Deep vs. shallow networks: An approximation theory perspective. *Analysis and Applications*, 14:829–848, 2016. <https://arxiv.org/abs/1608.03287>.
- [25] G. F. Montafur, R. Pascanu, K. Cho, and Y. Bengio. On the number of linear regions of deep neural networks. In *NIPS*, 2014. <https://arxiv.org/abs/1402.1869>.
- [26] R. Pascanu, T. Mikolov, and Y. Bengio. On the difficulty of training recurrent neural networks. In *ICML*, 2013. <https://arxiv.org/abs/1211.5063>.
- [27] J. Pennington, S. Schoenholz, and S. Ganguli. Resurrecting the sigmoid in deep learning through dynamical isometry: theory and practice. In *NIPS*, 2017. <https://arxiv.org/abs/1711.04735>.
- [28] J. Pennington and P. Worah. Nonlinear random matrix theory for deep learning. In *NIPS*, 2017. <https://papers.nips.cc/paper/6857-nonlinear-random-matrix-theory-for-deep-learning.pdf>.
- [29] G. Philipp, D. Song, and J. G. Carbonell. The exploding gradient problem demystified - definition, prevalence, impact, origin, tradeoffs, and solutions. In *arXiv preprint 1712.05577*, 2018. <https://arxiv.org/abs/1712.05577>.
- [30] B. Poole, S. Lahiri, M. Raghu, J. Sohl-Dickstein, and S. Ganguli. Exponential expressivity in deep neural networks through transient chaos. In *NIPS*, 2016. <https://arxiv.org/abs/1606.05340v1>.
- [31] M. Raghu, B. Poole, S. Ganguli, J. Kleinberg, and J. Sohl-Dickstein. On the expressive power of deep neural networks. In *ICML*, 2017. <https://arxiv.org/abs/1606.05336>.
- [32] A. M. Saxe, J. L. McClelland, and S. Ganguli. Exact solutions to the nonlinear dynamics of learning in deep linear neural networks. *ICLR*, 2014. <https://arxiv.org/abs/1312.6120>.
- [33] S. S. Schoenholz, J. Gilmer, S. Ganguli, and J. Sohl-Dickstein. Deep information propagation. In *ICLR*, 2017. <https://arxiv.org/abs/1611.01232>.
- [34] O. Shamir and R. Eldan. The power of depth for feedforward neural networks. *arXiv preprint arXiv:1512.03965*, 2015. <https://arxiv.org/abs/1512.03965>.
- [35] M. Telgarsky. Representation benefits of deep feedforward networks. *arXiv preprint arXiv:1509.08101*, 2015. <https://arxiv.org/abs/1509.08101>.
- [36] A. Veit, M. Wilber, and S. Belongie. Residual networks behave like ensembles of relatively shallow networks. In *NIPS*, 2016. <https://arxiv.org/abs/1605.06431>.
- [37] P. Wolfe. Convergence conditions for ascent methods. *SIAM Review*, 11(2):226–000, 1969. <https://epubs.siam.org/doi/pdf/10.1137/1011036>.
- [38] G. Yang and S. S. Schoenholz. Mean field residual networks: On the edge of chaos. In *NIPS*, 2017. <https://papers.nips.cc/paper/6879-mean-field-residual-networks-on-the-edge-of-chaos>.
- [39] G. Yang and S. S. Schoenholz. Deep mean field theory: Variance and width variation by layer as methods to control gradient explosion. In *ICLR workshop*, 2018. <https://openreview.net/forum?id=rJGY8GgR->.

A Architecture sampling

Each network layer is composed out of a fully-connected linear operation with bias and a nonlinearity operation. Some architectures have a normalization operation between the linear operation and the nonlinearity operation. The last layer does not contain the nonlinearity operation. Some architectures have skip connections, which always bypass two layers as in [16]. They start after either the linear operation or after the normalization operation. They end after the linear operation. The first skip connection begins after the linear or normalization operation in the first layer. The last skip connection ends after the linear operation in the last layer. All skip connections are identity skip connections, except the last skip connection, which has different input and output widths. The last skip connection multiplies the incoming signal with a $d_{L-2} \times d_L$ submatrix of a uniformly random $d_{L-2} \times d_{L-2}$ orthogonal matrix that is fixed throughout training.

Each architecture was selected independently at random via the following procedure.

- depth: Depth is chosen uniformly from the set of odd numbers between and including 3 and 49. We used odd numbers to avoid conflicts with our skip connections, which bypass blocks of two layers but do not bypass the first layer.
- width: Width was chosen automatically as a function of depth so that the number of trainable parameters in the network is approximately 1 million. The width of all layers except the input and output layer, which are determined by the data, is identical.
- linear operation: A $d_{l-1} \times d_l$ -dimensional weight matrix is initialized as a $d_{l-1} \times d_l$ -submatrix of a $\max(d_{l-1}, d_l) \times \max(d_{l-1}, d_l)$ uniformly random orthogonal matrix, multiplied by $\max(1, \sqrt{\frac{d_l}{d_{l-1}}})$. The advantages of orthogonal over Gaussian matrices have been documented by e.g. [4, 17, 28, 32]. We used the multiplicative factor so that the scale of the signal is preserved as it passes through the weight matrix, which is a well-accepted practice for avoiding exponential growth or decay in the forward pass used in e.g. He initialization [14] and SELU initialization [22]. With a 10% probability, we then additionally multiply all weight matrices by 0.9 and with a 10% probability, we multiply all weight matrices by 1.1. With a probability of $\frac{1}{\sqrt{2}}$, we initialize the trainable bias as a zero vector and with a probability of $1 - \frac{1}{\sqrt{2}}$, we initialize its entries as independent zero mean Gaussians with a variance of 0.05. We took the 0.05 value from [33]. If the bias is initialized as nonzero, we scale the weight matrix with a factor of $\sqrt{0.95}$ to approximately preserve the scale of the output.
- normalization: With a 50% probability, no normalization is used. With a 25% probability, batch normalization [20] is used. With a 25% probability, layer normalization [6] is used. Normalization does not use trainable bias and variance parameters.
- nonlinearity: We select one of the 8 nonlinearities shown in figure 2. We select ReLU, SeLU and Gaussian with probability $\frac{2}{11}$ each and tanh, even tanh, sigmoid, square and odd square with probability $\frac{1}{11}$ each. We downweighted the probabilities of tanh, even tanh and sigmoid as we considered them similar. The same holds for square and odd square. After choosing the initial nonlinearity, we added additional modifications. If the original nonlinearity is $\tau(s)$, we replace it by $c\tau(ds + t) + b$. First, d and t are chosen. d is 1 with probability 0.5, 1.2 with probability 0.25 and 0.8 with probability 0.25. t is 0 with probability 0.5, 0.2 with probability 0.25 and -0.2 with probability 0.25. Then, with probability $\frac{1}{\sqrt{2}}$, we set b so that if s follows a unit Gaussian distribution, $\tau(s)$ is unbiased, i.e. $\mathbb{E}_s \tau(s) = 0$. Therefore, the probability that both the bias of the fully-connected layer and bias of the nonlinearity in response to a unit Gaussian input is 0 is 0.5 overall. We set these probabilities to achieve a rough fraction of 50% unbiased architectures. Debiasing follows the example of [5]. Finally, we always set c so that if s is a unit Gaussian, then $\mathbb{Q}_s \tau(s) = 1$. Again, this follows the principle of avoiding exponential growth / decay in the forward pass as mentioned above. d , b , c and t are fixed throughout training.
- skip connections: With a 50% probability, no skip connections are used. With a 25% probability, skip connections of strength 1 are used, as is usually done in practice. With a 25% chance, the strength is set uniformly at random between 0 and 1. With a 50% chance, the skip connection starts after the linear operation. With a 50% chance, it starts after the

normalization operation. We introduced the latter variation because normalizing the signal between skip connections reduces the gradient damping of those connections for reasons related to the k -dilution principle [29]. We introduced both variations to obtain a more diverse range of NLCs amongst networks with skip connections.

After sampling, we conducted some mild post-processing. First, all networks that had square or odd square nonlinearities, or skip connections, that also did not have normalization were assigned either batch normalization or layer normalization with 50% probability each. This is, again, to avoid exponential instability in the forward pass. Second, if the bias of the linear layer was initialized to non-zero values and the network had batchnorm, we replaced batchnorm with layer norm, to avoid the bias being eliminated by batchnorm. Third, if the nonlinearity was not debiased, i.e. b was 0, and the nonlinearity is already debiased (i.e. SeLU, tanh and odd square), then we required the lateral shift t to be either 0.2 or -0.2 so that a bias would be introduced. This post-processing lead to the following changes in aggregate frequencies: no normalization - 20.5%, batchnorm - 28.1%, layer norm - 51.4%, lateral shift of nonlinearity - 55.3%.

We sampled 250 architectures for each of the three datasets. Results pertaining to those architectures are shown in figures 1, 2, 3A, 3C and 5. For the purpose of figure 3B, we edited our 250 architectures for CIFAR10 to increase bias. We replaced all instances of SeLU with ReLU, of tanh with sigmoid and of odd square with square. We always set b to zero, i.e. we did not debias nonlinearities. Finally, all instances of batchnorm were replaced by layer norm.

We used softmax+cross-entropy as the error function. Crucially, after initializing each architecture, we measured the scale c of activations fed into the error function, i.e. $c = \mathbb{Q}_{D,j} f_L(j)$. We then had the error function divide the incoming activations by c before applying cross-entropy. This was done so that the softmax+cross-entropy error function, which yields very different training dynamics when presented with inputs of different sizes, did not confound the outcomes of our study. We believe that that the preference of softmax+cross-entropy for outputs of a certain size has confounded the results of studies in the past. c remained fixed throughout training.

Finally, we note that we did not tweak our sampling procedure after training our networks, to avoid overfitting to the sampling procedure. We merely trained 20 architectures from a sampler that was only slightly different from the one described above. After observing the results, we tweaked the sampler to attain a more diverse range of NLC values as most of the 20 initial architectures had an NLC close to 1. Then we sampled our 750 architectures, 250 for each dataset, and did no further editing.

B Datasets

B.1 Selection

We wanted to conduct experiments on three different datasets. First, we chose MNIST and CIFAR10 as they are the two most popular datasets for evaluating deep neural networks. The MNIST dataset is composed of 28 by 28 black and white images of handwritten digits associated with a digit label that is between 0 and 9 [2]. The CIFAR10 dataset is composed of 32 by 32 color images of objects from 10 categories associated with a category label [1]. Unfortunately, due to the large number of training runs required for deriving robust conclusions and the resulting demand for computational resources, we were unable to replicate our results on ImageNet.

We decided to choose our third dataset from the UCI repository of machine learning datasets. [22] recently validated the SELU nonlinearity, which has since become popular, on a large number of datasets from this repository. We wanted to choose a dataset that [22] also used. To decide upon the specific dataset, we applied the following filters:

- The most frequent class should not be more than 50% more frequent than the average class.
- The dataset should contain between 1.000 and 100.000 datapoints.
- Datapoints should contain at least 10 features.
- The dataset should not be composed of images, as we already studied 2 image datasets.
- The dataset should not contain categorical or very sparse features.

- We only considered datasets that we were actually able to find on the repository website.

After applying all these filters, we were left with two datasets: waveform and waveform-noise. They are very similar. We chose the latter because of the greater number of input features. The waveform-noise dataset is composed of attributes of waves from three categories associated with a category label [3].

B.2 Processing

For waveform-noise, we normalized the mean and variance of the features. We processed CIFAR10 via the following procedure.

1. We normalize the mean and variance of each datapoint.
2. We normalize the mean of each feature.
3. Via PCA, we determine the number of dimensions that hold 99% of the variance. That number is 810.
4. We map each datapoint to an 810-dimensional vector via multiplication with a 3072×810 submatrix of a 3072×3072 uniformly random orthogonal matrix.
5. Finally, we multiply the entire dataset with a single constant so that we obtain $\mathbb{Q}_{\mathcal{D},j}x(j) = 1$.

We used the exact same procedure for MNIST, except that the number of dimensions of the final dataset was 334 instead of 810.

During preliminary experiments, we found that this pre-processing scheme lead to faster training and lower error values than training on the raw data where only the features are normalized. The reason we designed this scheme in the first place was to reduce input dimensionality so that the majority of our 1 million parameters would not reside in the first layer.

The MNIST dataset contains 60.000 training data points and 10.000 test data points. The training data was randomly split into a training set of size 50.000 and validation set of size 10.000. The CIFAR10 dataset contains 50.000 training data points and 10.000 test data points. The training data was randomly split into a training set of size 40.000 and a validation set of size 10.000. The waveform-noise dataset contains 5.000 data points, which were randomly split into a training set of size 3.000, a validation set of size 1.000 and a test set of size 1.000.

As mentioned, for CIFAR10, our input dimensionality was 810. For MNIST, it was 334. For waveform-noise, it was 40. For CIFAR10 and MNIST, the output dimensionality / number of classes was 10. For waveform-noise, it was 3.

C Experimental details

C.1 NLC illustration (table 1)

We use networks of the kind described in A with ReLU nonlinearities and no skip connections. The width was set to 100 and the bias initialized to zero. We compute the value for $GSC(0, L)$ empirically as $\frac{\mathbb{Q}_{\mathcal{D}}\|g_0\|_2 \mathbb{Q}_{\mathcal{D},i}f_0(i)}{\mathbb{Q}_{\mathcal{D}}\|g_L\|_2 \mathbb{Q}_{\mathcal{D},j}f_L(j)}$, where the expectation over \mathcal{D} is taken over the 50.000 training datapoints of the CIFAR10 dataset. Similarly, we compute $DBC(L)$ as $\frac{\mathbb{Q}_{\mathcal{D},j}f_L(j)}{\mathbb{Q}_j \mathbb{S}_{\mathcal{D}}f_L(j)}$ and $NLC(0, L)$ as $\frac{\mathbb{Q}_{\mathcal{D}}\|g_0\|_2 \mathbb{Q}_i \mathbb{S}_{\mathcal{D}}f_0(i)}{\mathbb{Q}_{\mathcal{D}}\|g_L\|_2 \mathbb{Q}_j \mathbb{S}_{\mathcal{D}}f_L(j)}$. We show the median across 10 random initializations, though the trends observed in figure 1 can be gleaned from any one of those initializations.

The color illustrations were produced as follows. We consider the same networks as before except we choose only a single random initialization, the input layer has width 100 instead of 810 and the output layer has width 3 instead of 10. We then generate three 100-dimensional inputs x^1, x^2 and x^3 by drawing from a Gaussian with mean zero and covariance I . Consider points (a, b, c) on the unit sphere in \mathbb{R}^3 . We associate each of these points with the input $ax^1 + bx^2 + cx^3$. Because each x^i is drawn from $\mathcal{N}(0, I)$, for each fixed tuple (a, b, c) , $ax^1 + bx^2 + cx^3$ also has marginal distribution $\mathcal{N}(0, I)$. We call the sphere of points associated with these inputs the “input sphere”.

For each of these inputs, we take the network we had previously initialized and propagate the input forward through the network. We obtain a 3-dimensional output at the prediction layer, which we divide by its length. Now the output lies on the unit sphere in \mathbb{R}^3 . Each point on that “output sphere” is associated with a color as shown in figure 6. Finally, we color each point on the input sphere according to its respective color on the output sphere.

All spheres are shown as azimuthal projections. The center of the depicted discs corresponds to the point $(\frac{\sqrt{3}}{3}, \frac{\sqrt{3}}{3}, \frac{\sqrt{3}}{3})$. The RGB values of colors on the output sphere are chosen so that the R component is largest whenever the first output neuron is largest, the G component is largest whenever the second output neuron is largest and the B component is largest whenever the third output neuron is largest. If we imagine that the prediction is fed into a softmax layer for 3-class classification, then “purer” colors correspond to more confident predictions.

All values were computed in the randomly initialized state. No training was conducted.

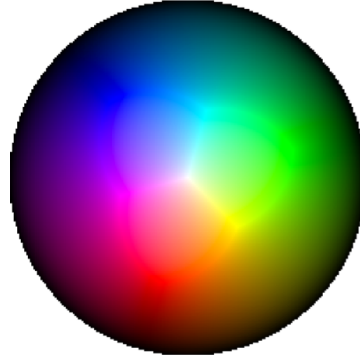


Figure 6: Coloring of the output sphere used for the illustrations in figure 1.

C.2 Gradient informativeness study (figure 1)

For each architecture, we consider a single random initialization. We divide each training set into batches of size 250. Let U be the uniform distribution over unit length vectors of dimensionality d_0 and let V be the uniform distribution over unit length vectors of dimensionality d_L . We measure the size of the maximum informative perturbation for each batch b as the largest value of ϵ such that if $actual := \mathbb{Q}_{D_b, u \sim U, v \sim V}(f_L(x + \epsilon \|x\|_2 u^T) - f_L(x))v$ and $grad_est := \epsilon \mathbb{Q}_{D_b, u \sim U, v \sim V} v^T \mathcal{J}_0^L u$, then $0.5actual \leq grad_est \leq 2actual$. In practice, \mathbb{Q} was evaluated by drawing a single u and v for each datapoint in the set of points in the b 'th batch D_b . Finally, we took the median across all batches.

The RGB value of each point plotted is determined as follows. The G value is zero. The R value, on a scale from 0 to 1, is $1 - \frac{1}{DBC(L)}$, where $DBC(L)$ was computed as before. The B value, on a scale from 0 to 1, is equal to the strength of the skip connections. Specifically, it is zero if there are no skip connections.

All values were computed in the randomly initialized state. No training was conducted.

C.3 Predictiveness study (figures 2, 3 and 5)

For each architecture, we considered a single random initialization. Given computational budget constraints, we preferred running a larger number of architectures versus re-running the same architecture with different initializations. We trained them with SGD using batch size 250. To ensure that there is no bias with regards to step size, we tuned the step size independently for each architecture by conducting a large number of training runs for each architecture. A training run is conducted as follows. We train with the starting step size until the validation classification error (VCE) has not decreased for 10 epochs. Then we rewind the state of the network by 10 epochs (when the lowest VCE was achieved), divide the step size by 3 and continue training until the validation classification error has not improved for 5 epochs. We divide the step size by 3 again, rewind and continue training until the validation classification error has not improved for 5 epochs. This process continues until the step size has been divided by 3 ten times.

The first training run for each architecture was conducted with a small starting step size. We then keep multiplying the starting step size by 3 until at least 7 training runs are conducted and the final VCE has not improved for at least 2 training runs (MNIST / CIFAR10) or 4 training runs (waveform-noise). The starting step size which achieved the lowest VCE was then selected for presentation in this paper. The test classification error shown is computed after the final rewind operation, at the epoch where the achieved VCE was lowest. $NLC(0, L)$ is computed in the initialized state as in section C.1.

In figure 2, points are colored as in figure 1 as described in section C.2. In figure 3B, the R value, on a scale from 0 to 1, is equal to $1 - \frac{1}{\max(NLC(0, L), 1)}$. In figure 3A, ‘ $NLC(0, L)$ post-training’ was

taken at the same epoch the test classification error was taken. In figure 3C, the architectures were trained by Adam instead of SGD, but the step size search procedure was the same.

C.4 Approximability study (table 2)

$NLC_\tau(1)$ was computed as defined in section 5. $NLC_\tau(1)^{48}$ is simply the exponentiated value. The linear approximation error is computed as $(\frac{\mathbb{Q}_{s \sim \mathcal{N}(0,1)} \tau(s) - \bar{\tau}(s)}{\mathbb{Q}_{s \sim \mathcal{N}(0,1)} \bar{\tau}(s)})^2$, where $\bar{\tau}$ is the best linear fit to τ for inputs drawn from $\mathcal{N}(0, 1)$, i.e. $\arg \min_{\bar{\tau} \text{ linear}} \mathbb{Q}_{s \sim \mathcal{N}(0,1)} \tau(s) - \bar{\tau}(s)$. Finally, $NLC(0, L)$ for batchnorm networks was computed as in section C.1. We present the median across 10 random initializations. The values for different initializations do not vary much except for the square and odd square nonlinearities for reasons stated in the main text.

C.5 Robustness study (figure 4)

We used a single ReLU network with batch normalization as in section C.1, of depth 10. We multiply the weights with factor 10^7 and initialize the biases with standard deviation 10^{10} . Note that these large values are chosen purely for illustrative purposes.

$NLC(l, L)$ was computed as $\frac{\mathbb{Q}_{\mathcal{D}} \|g_l\|_2 \mathbb{Q}_i \mathbb{S}_{\mathcal{D}} f_l(i)}{\mathbb{Q}_{\mathcal{D}} \|g_L\|_2 \mathbb{Q}_j \mathbb{S}_{\mathcal{D}} f_L(j)}$. $GVC S(l)$ was computed as $\mathbb{Q}_{j, \mathcal{D}} f_l(j)$ and the correlation of two uncorrelated inputs was approximated by the expected correlation of two independently chosen inputs from $\mathcal{N}(0, 1)$, which was further approximated by $DBC(l)$.

All values were computed in the randomly initialized state on CIFAR10. No training was conducted.